

Study of the Normal Force and Velocity Influence on the Fused Silica Scratching Mechanisms with α -Alumina Grit at Atomic Scale via Reaxff Reactive Molecular Dynamic Simulations

Juan I. Ahuir-Torres^a, Xun Chen^a, Luke Mason^b, Philippe Gambron^b, David D. Walker^c, Guoyu Yu^c, Hongyu Li^c, Rakesh Mishra^d, Yasemin Akar^d, Frankie F. Jackson^d, Paul A. Bingham^f

^a General Engineering Research Institute, Faculty of Engineering and Technology, Liverpool John Moores University, GERI Building, 3 Byrom Street, Liverpool, Merseyside, L3 3AF, United Kingdom.

^b Scientific Computing Department, Science and Technology Facilities Council, North Star Avenue, Swindon, Wiltshire, SN2 1SZ, United Kingdom.

^c SciTech Daresbury National Science & Innovation Campus, University of Huddersfield Laboratory for Ultra Precision Surface, G6 TechSpace One Keckwick Lane, Daresbury, Merseyside, WA4 4AB, United Kingdom.

^d Department of Engineering and Technology, School of Computing and Engineering, University of Huddersfield, Huddersfield, West Yorkshire, HD1 3DH, United Kingdom.

^e College of Business, Technology and Engineering, Sheffield Hallam University, City Campus, Howard Street, Sheffield, South Yorkshire, S1 1WB, United Kingdom.

Abstract: The fused silica is an optical glass material employed in several industries, which is usually grinded and polished to obtain an ultra-smooth surface. α -alumina is often employed to get this surface. The scratching testing is a powerful technique to assess the process conditions that provoke the process induced damages. Normal force applied on abrasives and sliding velocity are main parameters to be considered in the scratching testing. Although the scratching mechanical mechanisms of the fused silica have previously been studied in depth, its chemical mechanisms have poorly been analysed. In this paper, the Reaxff reactive molecular dynamic simulation is used to study these mechanical and chemical mechanisms in various scratching processes under different velocities and normal loads. The results showed dissimilar types of scratching (penetration, penetration with dragging and dragging) according to the velocity and normal force. The scratching depth was higher at larger normal force and slower velocity. The temperature and potential energy also were stable at low normal force and slow velocity. The chemical interaction between the grain and the optical glass material furthermore appears as the adhesion.

Nomenclature

- SiO₂; Silica
- MD; Molecular dynamic
- SiC; Silicon carbide
- LAMMPS; Large-scale atomic/molecular massively parallel simulator
- Ce; Cerium
- Si; Silicon
- O; Oxygen
- R; Material block
- H; Hydrogen
- Al; Aluminium
- Cu; Copper
- C; Carbon
- COF; Fiction coefficient
- QM; Quantum mechanics
- E_{Total}; Total energy
- E_b; Bond energy
- E_a; Atomic energy
- E_{lp}; Lone pair energy
- E_{CO}; Valence angle conjugation energy
- E_T; Torsion energy
- E_V; Valence angle energy
- E_c; Coulomb energy
- E_W; Van der Waals energy
- E_H; Hydrogen energy
- p_{bo,1}; Bond term for first electron
- p_{bo,2}; Bond term for second electron
- p_{bo,3}; Bond term for third electron
- p_{bo,4}; Bond term for fourth electron
- p_{bo,5}; Bond term for fifth electron
- p_{bo,6}; Bond term for sixth electron
- r_{ij}; Interatomic distance
- r_o^σ; Equilibrium length for the sigma bond
- r_o^π; Equilibrium length for the first pi bond
- r_o^{ππ}; Equilibrium length for the second pi bond
- D_c; Dissociation energy
- p_{be,1}; Empirical parameter
- p_{be,2}; Empirical parameter

- p_a ; Atom term
- Val ; Number of valence electrons
- λ_a ; Experimental term of the atomic coordination
- p_{lp} ; Lone pair term
- $n_{lp,opt}$; Optimum lone pair electron number
- $n_{lp,i}$; Lone pair electron number
- $f_1(BO_{i,j}, BO_{j,k}, BO_{k,l})$; Resonance or conjugation function
- p_{CO1} ; First conjugation term
- w_{ijk} ; Torsion angle
- θ_{ijk} ; Angle formed between first second and third atoms
- θ_{jkl} ; Angle formed between second, third and fourth atoms
- p_{CO2} ; Second conjugation term
- $BO_{i,j}$; Order of the bond for first and second atoms
- $BO_{j,k}$; Order of the bond for second and third atoms
- $BO_{k,l}$; Order of the bond for third and fourth atoms.
- $f_2(BO_{i,j}, BO_{j,k}, BO_{k,l})$; Function of the torsion smooth disappearance
- K_1 ; Force constant for second and third atoms
- p_{T1} ; First torsion term
- K_2 ; Force constant for third and fourth atoms
- p_{T2} ; Second term
- $f_3(\Delta_i, \Delta_j)$; Function of the lone pair electrons on torsion
- λ_{T1} ; First experimental parameter of the torsion
- BO_j ; Bond order for second atom
- Val_j ; Valence of second atoms
- BO_k ; Bond order of third atom
- Val_k ; Valence of third atom
- λ_{T2} ; Second experimental parameter of the torsion
- p_{V1} ; First valence angle term
- $f_4(BO_{i,j})$; Function of the valence angle of the first and second angle
- $f_5(BO_{j,k})$; Function of the valence angle of the second and third angle
- $f_6(\Delta_j)$; Function of the second atom lone pair electron on the valence angle
- p_{V2} ; Second term of the valence angle
- θ_0 ; Equilibrium valence angle
- p_{V3} ; Third valence angle term
- p_{V4} ; Fourth valence angle term
- p_{V5} ; Fifth valence angle term
- p_{V6} ; Sixth valence angle term
- BO_j ; Radius function for the second atoms
- p_{V7} ; Seventh valence angle term
- C ; Coulomb constant

- q_i ; First atomic charge
- q_j ; Second atomic charge
- $r_{i,j}$; Interatomic distance
- $\gamma_{i,j}$; Shielding parameter
- $D_{i,j}$; Polarisation dissociation
- $\alpha_{i,j}$; Polarisation factor
- $f(r_{i,j})$; Shield interaction function
- r_w ; Van der Waals radius
- p_w ; Van der Waals term
- γ_w ; Van der Waals shielding parameter.
- p_{H1} ; First hydrogen bond parameter
- p_{H2} ; Second hydrogen bond parameter
- p_{H3} ; Third hydrogen bond parameter
- BO_{XH} ; Hydrogen bond order
- r_H^0 ; Equilibrium hydrogen bond
- r_{ZH} ; Distance between the hydrogen and the atom
- θ_{XHZ} the angle between the hydrogen and the atom
- Al^{+3} ; Aluminium cation (+3)
- O^{-2} ; Oxygen anion (-2)
- Si^{+4} ; Silicon cation (+4)
- COF; Coefficient of friction
- F_N ; Normal force or load
- V ; Horizontal or sliding velocity
- NVT; Canonical ensemble
- NVE; Microcanonical ensemble

Introduction

The fused silica (amorphous SiO_2) is the base of the optical glass materials that are used in several fields as, laser, telecommunications, astrophysics and optics [1-3]. The optical glass material must have a surface with low roughness that is created via grinding, lapping and polishing processes [4-6]. α -alumina is one of the principal materials used as abrasives in these processes [7-10]. The optical glass material can however be damaged during these processes [4, 8, 11]. Scratching testing is a great technique to analyse the mechanical properties and the integrity of the optical glass materials [3, 11-13], and has been employed to analyse the formation mechanisms of these damages. The scratching normal force and scratching velocity are considered to be main influential factors in association with the damage formation that starts to occur at atomic scale [2, 3, 13]. Moreover, the chemical interactions between the interactive materials could be important factors that affect the damage formation mechanisms at nanoscale. The direct study of these mechanisms and

interactions at atomic scale via experimental assessments, is currently impossible because the intrinsic difficulty at such a small scale. Molecular dynamic (MD) simulation can be a good method to carry out this study [14-17].

The molecular dynamic simulation is a semi-empirical method that allows to define the trajectory of the atoms and molecules via numerically Newton's equations of motion for a system of the interacting particles. The force and the potential energy of the atoms and molecules are calculated via using atomic and molecular force fields [18, 19]. Thus, MD is a great method to evaluate the physical and chemical interactions between materials at nanoscale, which has been employed to simulate the scratching processes at various conditions. In 2016, Han [18] reported his investigation of the mechanical and chemical interactions in a silica glass mechanical polishing via MD. The research assessed the mechanical and chemical interaction of a particle when impacts on the block surface. Tian et al [17] studied the scratching at atomic scale of the two silicon carbide (4H-SiC and 6H-SiC) with MD simulator code, large-scale atomic/molecular massively parallel simulator (LAMMPS). The Tersoff potential was used to simulate the covalent bonds and, the scratching velocity and depth were 100 m/s and 5 nm, respectively. This study showed that the 6H-SiC and 4H-SiC own similar properties except that the normal resistance is higher for 4H-SiC. Later, Tian et al [20] investigated the scratching depth influence on the materials and illustrated that the amorphous transformation and the dislocations are the main mechanisms of material removal. The specific energy of cutting moreover is lower at deeper penetrations Meng et al [21] also studied the sliding velocity influence on scratching process of the silicon carbide with diamond tool at constant depth via MD using LAMMPS. In this case, the silicon carbide was 3C-SiC, the potential field was ABOP potential, tool shape was pyramid, depth was 3 nm and the scratching velocities was from 10 m/s to 200 m/s. Meng et al determined that the fast velocities cause lower dislocations than the slow speeds because the lower hydrostatic stress. Zhang et al [22] carried out the study of the diamond scratching on copper with double tools through MD-LAMMPS. The potential field was EAM potential, the velocity was 100 m/s and a pyramid tool was used. Various tool position effects on scratching were evaluated in this paper and the parallel tool scratching generates the grooves with the best quality. Recently, Wu et al [23] conducted a similar simulation on 6H-SiC, with spherical tools at 20 m/s scratching speed and 2 nm of the depth. The plastic deformation of the material was considered as a result of the amorphization and dislocation activity. The double scratching at short distance between grains moreover provokes the new crystalline structure generation in the zone between scratching owing to the high temperature and stress in this zone.

Shi et al [24] carried out a study about the chemical interactions of a diamond polishing with diamond in water environment at several velocities and normal forces via the simulation and experimental analyses. The simulations were conducted via MD-LAMMPS with Reaxff field as potential field. The hydroxide peroxide was included in the water in the experimental and simulation tests. The increasing of the normal force enlarges the coefficient friction (COF) owing the enlargement of the C-O-C bond number generations. The following three cases are examples: (1) 488 nN F_N , 0.08 COF and 0 C-O-C bonds; (2)

1736 nN F_N , 0.1 COF and 9 C-O-C bonds; (3) 2783 nN F_N , 1.15 COF and 51 C-O-C bonds. The addition of the hydroxide peroxide in the water also reduces the friction force from 200nN to 150nN. This is due the chemical reaction of oxygen, hydrogen and hydroxyl of the hydrogen peroxide degradation with the carbon hinders the production of C-O-C bonds. The research group of Gou et al [25] studied the pressure influence on polishing process of the silica with silica trough using similar simulation conditions as Shi. The material removal ratio is increased through the generation of the hydroxyl compounds on the silica that allows the production of the chemical bonds between bodies. The material removal is larger with hydrogen peroxide at 30% (13 molecules of silica) than only with water (6 molecules of silica) owing to this chemical compound is a catalyser of the hydroxyl group on silica. The increasing of the pressure moreover provokes more chemical bonds between body molecules. Onodera et al [26] assessed the effects of the normal force on the chemical reactions between α -quartz, water and ceria in a polishing process. Ondera et al observed that the chemical reaction between ceria and silica produces Ce-O-Si-R bonds that weaken the bonds between the silica molecules of the block. Thus, this chemical reaction eases the silica removal form the block. Other study via MD simulation of the chemical influence on the mechanical process was carried out by Wen et al [27], which was about the amorphous silica polishing with abrasive powder (α -quartz) in water. The potential field Reaxff was used. The research revealed that the α -quartz silica molecules generate bonds with amorphous silica molecules are the main material removal mechanism. The hydroxide peroxide furthermore eases the formation of these bonds and increases the friction force.

Although the scratching processes have widely been studied, these were only focused on the mechanical and physical part. Also, the chemical part of the polishing has deeply been evaluated through simulations in water environment but the simulation analyses in dry conditions are scare. The study of the chemical part of the scratching process in dry conditions thus is null. For this reason, this paper presents the physical and chemical phenomena under the variation of normal force and velocity of scratching processes on fused silica with α -alumina as abrasive grain or tool. The Reaxff field was used as potential field in this study to simulate the chemical reactions in scratching process because this allows to simulate the generation, breaking and replace of the chemical bonds (e.g. covalent, ionic, metallic and macromolecular) [28]. Other force fields method only permits to simulate the bonds and their interaction for each other but the bond generation and breaking simulations are limited.

Method and models

1. Methods and general conditions

MD is a semi-empirical method to simulate the atom interactions and velocities through newton's equation. Here the MD simulations were carried out using LAMMPS software [29]. The force fields were simulated via Reaxff method with H/O/Si/Al/Cu force field [30].

The Reaxff method permits to model the chemical interaction and reaction by means of the simulation of the chemical bond breaking and generation. All simulations were conducted with real units (defined in LAMMPS), in 3 dimensions with f p f boundary, full atom style and with 3.0 bin of neighbour. Here the f p f boundary features of the global simulation box indicate the boundary in X and Z directions are fixed (f letter) while the boundary in Y direction is periodic (p letter) and allowed the interaction between sides. Here the radius of the interaction between atoms is function of the Reax force field plus 0.3 nm according to 3.0 bin and real unit (defined in LAMMPS). The simulation were visualised through Ovito software [31].

2. Reactive force-field (Reaxff) interatomic potential

The reactive force-field (ReaxFF) interatomic potential is a powerful computational tool for materials interactions based on the principles of quantum mechanics (QM). The force field Reaxff allows to simulate the chemical interactions by means of the representation of the bond breaking, generating and replacing. The total energy of the system (E_{Total}) could be estimated via the chemical characteristics via this force field, as presented in equation (1) [32, 33].

$$E_{Total} = E_b + E_a + E_{lp} + E_{CO} + E_T + E_V + E_C + E_W + E_H \quad (1)$$

Where, E_b is the bond energy, E_a is the atomic energy, E_{lp} is the lone pair energy, E_{CO} is the valence angle conjugation energy, E_T is the torsion energy, E_V is the valence angle energy, E_C is the coulomb energy, E_W is the Van de Waals energy and E_H is the hydrogen energy. The majority of these energies are functions of the bond order (e.g. single, double or triple) that is represented as equation (2) [32-35].

$$BO_{j,i} = \exp \left[p_{bo,1} * \left(\frac{r_{ij}}{r_0^\sigma} \right)^{p_{bo,2}} \right] + \exp \left[p_{bo,3} * \left(\frac{r_{ij}}{r_0^\pi} \right)^{p_{bo,4}} \right] + \exp \left[p_{bo,5} * \left(\frac{r_{ij}}{r_0^{\pi\pi}} \right)^{p_{bo,6}} \right] \quad (2)$$

Being, $p_{bo,1}$ the bond term for first electron, $p_{bo,2}$ the bond term for second electron, $p_{bo,3}$ the bond term for third electron, $p_{bo,4}$ the bond term for fourth electron, $p_{bo,5}$ the bond term for fifth electron, $p_{bo,6}$ the bond term for sixth electron, r_{ij} the interatomic distance, r_0^σ the equilibrium length for the sigma bond, r_0^π the equilibrium length for the first pi bond and $r_0^{\pi\pi}$ the equilibrium length for the second pi bond [35].

The bond energy E_b is defined by order (e.g. single, double or triple) force, number and length of the chemical bonds as in equation (3) [32-35].

$$E_b = \sum_{j=1}^{i=bon \ number} -D_e * BO_{j,i} * \exp \left[p_{be,1} * \left(1 - B_{i,j}^{p_{be,2}} \right) \right] \quad (3)$$

where, D_e is the dissociation energy, $p_{be,1}$ and $p_{be,2}$ are empirical parameters [35].

The atomic energy E_a is determined by the electron around atoms that are the non-bonding and bonding electrons. This chemical parameter thus indicates the atomic coordination (bond number) of the molecule. E_a is therefore called as over and under coordination energy. The function of this energy can be found in the equation (4) [36].

$$E_a = p_a * (BO_{i,j} - Val_i) * \left(\frac{1}{1 + \exp(\lambda_a * (BO_{i,j} - Val_i))} \right) \quad (4)$$

Where, p_a is the atom term, Val is the number of valence electrons and λ_a is experimental term of the atomic coordination.

The non-bonding (lone pair) electrons number defines the E_{lp} as can be seen in the equations (5) and (6) [32].

$$n_{lp,i} = \text{int}\left(\frac{BO_{i,j} - Val_i}{2}\right) + \exp\left[-p_{lp} * (BO_{i,j} - Val_i + 2 - \text{int}\left(\frac{BO_{i,j} - Val_i}{2}\right)^2)\right] \quad (5)$$

$$E_{lp} = \frac{p_{lp} * (n_{lp,opt} - n_{lp,i})}{1 + \exp(-75 * (n_{lp,opt} - n_{lp,i}))} \quad (6)$$

Being, p_{lp} the lone pair term, $n_{lp,opt}$ the optimum lone pair electron number and $n_{lp,i}$ the lone pair electron number.

E_{CO} is defined by the resonance of the electrons on the molecules that is determined by the order of bonds as can be viewed in the equations (7) and (8) [32].

$$E_{CO} = f_1(BO_{i,j}, BO_{j,k}, BO_{k,l}) * p_{CO1} * (1 + (\cos^2(w_{iljk}) - 1) * \sin \theta_{ijk} * \sin \theta_{jkl}) \quad (7)$$

$$f_1(BO_{i,j}, BO_{j,k}, BO_{k,l}) = \exp[-p_{CO2} * ((BO_{i,j} - 1.5)^2 + (BO_{j,k} - 1.5)^2 + (BO_{k,l} - 1.5)^2)] \quad (8)$$

Where, $f_1(BO_{i,j}, BO_{j,k}, BO_{k,l})$ is the resonance or conjugation function, p_{CO1} is the first conjugation term, w_{iljk} is the torsion angle, θ_{ijk} is the angle formed between first, second and third atoms, θ_{jkl} is the angle formed between second, third and fourth atoms, p_{CO2} is the second conjugation term, $BO_{i,j}$ is the order of the bond for first and second atoms, $BO_{j,k}$ is the order of the bond for second and third atoms and $BO_{k,l}$ is the order of the bond for third and fourth atoms.

The mobility freedom of the molecule is the main factor in E_T , whose function can be found in equations (9), (10) and (11) [36].

$$E_T = f_2(BO_{i,j}, BO_{j,k}, BO_{k,l}) * \sin \theta_{ijk} * \sin \theta_{jkl} * \left[\frac{1}{2} * K_1 * \exp(p_{T1} * \right.$$

$$(BO_{j,k} - 3 + f_3(\Delta_j, \Delta_k)^2) * (1 - \cos 2 * w_{ijkl}) + \frac{1}{2} * K_2 * (1 + \cos 3 * w_{ijkl}) \quad (9)$$

$$f_2(BO_{i,j}, BO_{j,k}, BO_{k,l}) = [1 - \exp(-p_{T2} * BO_{i,j})] * [1 - \exp(-p_{T2} * BO_{j,k})] * [1 - \exp(-p_{T2} * BO_{k,l})] \quad (10)$$

$$f_3(\Delta_i, \Delta_j) = \frac{2 + \exp[-\lambda_{T1} * (BO_j - Val_j + BO_k - Val_k)]}{1 + \exp[-\lambda_{T1} * (BO_j - Val_j + BO_k - Val_k)] + \exp[\lambda_{T2} * (BO_j - Val_j + BO_k - Val_k)]} \quad (11)$$

Being, $f_2(BO_{i,j}, BO_{j,k}, BO_{k,l})$ the function of the torsion smooth disappearance, K_1 the force constant for second and third atoms, p_{T1} the first torsion term, K_2 the force constant for third and fourth atoms, p_{T2} the second term, $f_3(\Delta_i, \Delta_j)$ the function of the lone pair electrons on torsion, λ_{T1} the first experimental parameter of the torsion, BO_j the bond order for second atom, Val_j the valence of second atoms, BO_k the bond order of third atom, Val_k the valence of third atoms and λ_{T2} the second experimental parameter of the torsion.

The valence angle (molecular angle) defines E_V , which can be seen in equations (12), (13), (14) and (15) [32].

$$E_V = -p_{V1} + f_4(BO_{i,j}) * f_5(BO_{j,k}) * f_6(\Delta_j) * [p_{V1}(1 - \exp(-p_{V2} * (\theta_o(BO) - \theta_{ijk})^2))] \quad (12)$$

$$f_4(BO_{i,j}) = 1 - \exp(-p_{V3} * BO_{ij}^{p_4}) \quad (13)$$

$$f_5(BO_{j,k}) = 1 - \exp(-p_{V3} * BO_{jk}^{p_4}) \quad (14)$$

$$f_6(\Delta_j) = p_{V5} - (p_{V5} - 1) * \frac{2 + \exp(p_{V6} * (BO_j - Val_j))}{1 + \exp(p_{V6} * (BO_j - Val_j)) + \exp(-p_{V7} * (BO_j - Val_j))} \quad (15)$$

Where, p_{V1} is the first valence angle term, $f_4(BO_{i,j})$ is the function of the valence angle of the first and second angle, $f_5(BO_{j,k})$ is the function of the valence angle of the second and third angle, $f_6(\Delta_j)$ is the function of the second atom lone pair electron on the valence angle, p_{V2} is the second term of the valence angle, θ_o is the equilibrium valence angle, p_{V3} is the third valence angle term, p_{V4} is the fourth valence angle term, p_{V5} is the fifth valence angle term, p_{V6} is the sixth valence angle term, BO_j is the radius function for the second atoms and p_{V7} is the seventh valence angle term.

The charge of the atoms and the interatomic distance are parameters that define E_C , as being indicated in the equation (16) [33].

$$E_C = \frac{C * q_i * q_j}{(r_{i,j}^3 + (\frac{1}{\gamma_{i,j}})^3)^{1/3}} \quad (16)$$

Being, C the coulomb constant, q_i the first atomic charge, q_j the second atomic charge, $r_{i,j}$ the interatomic distance and $\gamma_{i,j}$ the shielding parameter.

E_W is determined via the distance between atoms and the polarizability how can be seen in the equations (17) and (18) [32, 36].

$$E_W = D_{i,j} * \left[\exp\left(\alpha_{i,j} * \left(1 - \frac{f(r_{i,j})}{r_w}\right)\right) - 2 * \exp\left(\frac{\alpha_{i,j}}{2} * \left(1 - \frac{f(r_{i,j})}{r_w}\right)\right) \right] \quad (17)$$

$$f(r_{i,j}) = [r_{i,j}^{p_w} + \left(\frac{1}{\gamma_w}\right)^{p_w}]^{1/p_w} \quad (18)$$

Where, $D_{i,j}$ is the polarisation dissociation, $\alpha_{i,j}$ is the polarisation factor, $f(r_{i,j})$ is the shield interaction function, r_w is the Van der Waals radius, p_w is the Van der Waals term and γ_w is Van der Waals shielding parameter.

The hydrogen energy E_H is defined by the force, angle and number of the hydrogen bond as showing in equation (19) [32].

$$E_H = p_{H1} * [1 - \exp(p_{H2} * BO_{XH})] * \exp\left[p_{H3} * \left(\frac{r_H^o}{r_{ZH}} + \frac{r_{ZH}}{r_H^o} - 2\right)\right] * \left(\sin \frac{\theta_{XHZ}}{2}\right)^8 \quad (19)$$

Being, p_{H1} , p_{H2} and p_{H3} the first, second and third hydrogen bond parameter, BO_{XH} the hydrogen bond order, r_H^o the equilibrium hydrogen bond, r_{ZH} distance between the hydrogen and the atom and θ_{XHZ} the angle between the hydrogen and the atom. This energy is only observable for systems with water, hydrofluoridric acid or/and hydroxyl/alcohol groups.

Note, E_C , E_W and E_H are non-bonding energies while E_b , E_a , E_{CO} , E_{lp} , E_T and E_V are bonding energies.

3. Simulated Materials and model setup

Two materials were used to conduct the scratching simulations, which were the grain and optical glass material. The sketch of the system can be observed in Figure 1.

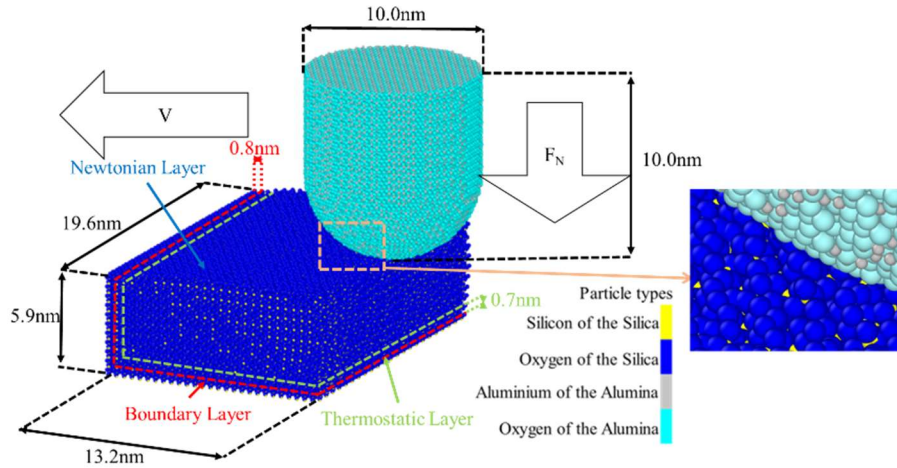


Figure.1. MD simulation system consisted of fused silica (optical glass) and α -alumina (grain).

In the simulation, the grain was the tool to scratch the optical glass material surface. The material of the grain was α -alumina formed by Al^{+3} and O^{-2} with hexagon packaged closed (HPC) [37]. The partial charges of the elements were $-1.0158 e^-$ for oxygen and $1.5237 e^-$ aluminium [38]. The shape of the grain was a cylinder with a semi-spherical base. The height of the cylinder was 5 nm and the radius of the 5 nm. The grain was designed as hollow rigid body with 1 nm of thickness to reduce the computing time [17].

The optical glass material was α -quartz [25] consisted of the Si^{+4} and O^{-2} , whose partial charges were $2.4000 e^-$ and $-1.2000 e^-$ [39], respectively. The size of the optical glass material block was 13.2 nm x 19.5 nm x 5.9 nm in X, Y and Z axes. The glass block was formed of three layers to stabilise the simulation [17, 40], which were the next:

- Boundary layer was placed in the bottom and X axis right side of the block and its thickness was 0.8 nm. The atoms of this layer were set to remain a constant position during the simulation to represents the part of the optical glass material outside the scratched zone.
- Thermostatic layer was top and left of the boundary layer, whose thickness was 0.7 nm. This layer was used to simulate the dissipation heat into the bulk material by mean of thermal conductivity. This was conducted via Berendsen thermostat for temperature simulation and canonical ensemble (NVT) for the atom trajectory and velocity.
- Newtonian layer was the last layer that was the rest of the block, which represents the scratching zone where the abrasive grain interacted with the optical glass material. The velocity and trajectory of the atoms for this layer was simulated via microcanonical ensemble (NVE).

The grain was localised to the left side of the X axis, in the middle of the Y axis and on the optical glass material surface.

4. Process Conditions for Scratching Simulation

The assembled atom system was initialised and stabilised for 40 ps before the normal force (F_N) in Z direction and horizontal velocity (V) in X direction were applied on abrasive grain. In the simulation, the F_N that represented normal polishing load on grains varied at different levels as 0.05 nN, 0.75 nN, 3.00 nN, 10.00 nN, 40.00 nN and 80.00 nN while the V were selected as 10 m/s and 100 m/s.

Results and Discussion

1. Physical Phenomena

This section presents and discusses the physical characteristics of the scratching simulation. These features under consideration are the optical glass material temperature and potential energy development over time, the type, depth and displacement of the scratching. These observations and discussions are essential to understand the scratching physical processes and the stability of the system.

The optical glass material temperature and the potential energy of the system development over time are the first characteristics to be assessed, which can be observed in Figure 2. The temperature (Fig.2. a, b) owned a dissimilar behaviour with the time according to the normal force and sliding velocity. The simulations nevertheless showed a temperature could have a short period staying at a relatively constant level, then elevated gradually toward a stage where the temperature increased drastically, which indicated glass melted and the system was instable.

The simulations at 100m/s scratching speed with normal load ≥ 10.00 nN (Fig.2.a) shows the temperature remained constant until the destabilisation point. This is due to both the friction energy [41] and the bond breaking via scratching pressure [42, 43] that increase the temperature of the system. The simulations at 100 m/s scratching speed with normal load ≤ 3.00 nN showed similar temperature evolution to the previous simulation at first 10 picoseconds (≈ 10 ps). After this point, the temperature progressively elevated with the time until the system destabilisation point. This increment also is because the friction and removal material [41-43] but, these processes are less drastic than that for the previous case.

The temperature variation over time in the simulation at the scratching speed of 10 m/s and the normal load ≥ 10.00 nN (Fig.2.b) was similar to that under the scratching speed of 100 m/s with the same normal load. The simulation results with normal loads at 3.00 nN and 0.75 nN showed similar slow temperature elevation as those with higher normal forces up to 16 ps. The temperature elevation slowed down after this point because of the heat rate and the dissipation heat begin to be in equilibrium. The destabilisation of the system was found when the temperature dramatically increased. The simulation at the scratching speed of 10 m/s under normal load 0.05 nN possessed a similar temperature elevation as other normal loads up to 80 ps (Fig.2.b. black curve). After this point, the temperature remained fairly stable with slightly increase over the time up to 208 ps. This stable temperature

indicates that the heating rate is similar to the heat dissipation rate. The last part of the temperature evolution was characterised by a temperature peak from 208 ps to 256 ps due to a large amount of material displacement – a phenomenon of dragging. The material displacement is the main removal mechanism for dragging that breaks the silica block bonds via silica adhesion on α -alumina. The breaking of the bonds commonly is an exothermic reaction that raises the temperature [42]. This was observed as the up slope of the peak. The re-localisation of the material passed contact area on surface then generates new bonds between detached silica and optical glass material surface. The bond production commonly is an endothermic process that reduces the temperature [42]. These processes were also observed in the chemical phenomena that will be discussed further later.

The dissimilar development of temperature over time according to velocity is because friction energy is proportional to this factor [41, 45].

The potential energy developments over time (Fig.2.c,d) were inversely similar to that of the temperature evolutions. This is because the potential energy represents the stability of the system (atom immobility) that is opposite feature to the temperature.

The loss of the kinetic energy during scratching is converted to friction energy [46]. The excessive friction energy could massively break the chemical bonds of the optical glass material. The massive breaking of the chemical bonds permits to have more movement freedom to the molecules and atoms. The temperature only is a representation of the molecular/atomic movement [47]. High temperatures therefore showed molecules and atoms with fast speed. The bond breaking also is an exothermic process that supplies an extra temperature to system [42]. The time to reach this destabilisation system was longer at slower velocity and lower normal force. This is owing to the friction energy is proportional to sliding velocity [46] and normal force [48].

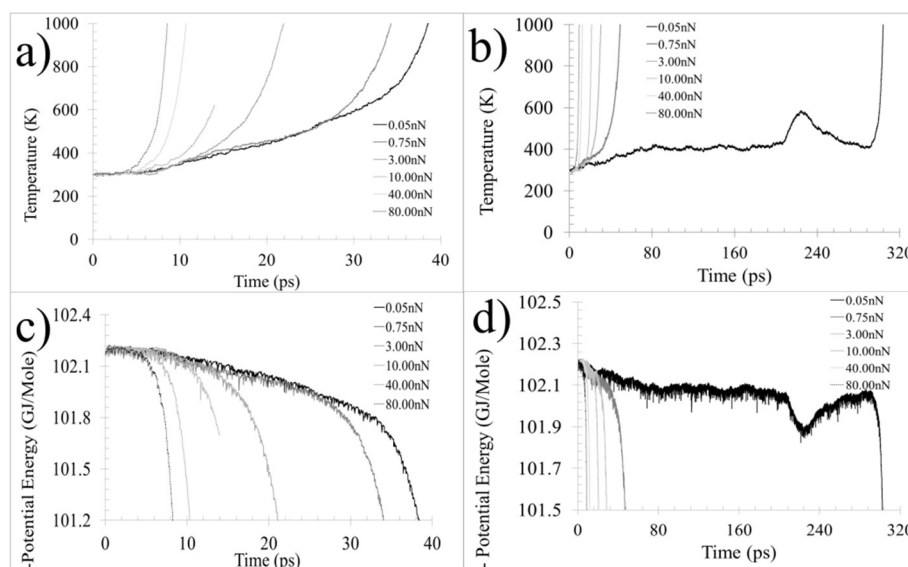


Figure.2. Variation of temperature and potential energy in the scratching of optical glass at 100m/s (a, c) and 10 m/s (b, d).

The behaviours of scratching processes just before the destabilisation of the system can be visualised in Figure 3. Three types of the scratching actions were observed according to normal force and velocity, which were penetration, penetration with dragging, and dragging.

The first type of the scratching is penetration as illustrated in Fig.3. (a, b, d), which happened in the scratching processes at the speed of 100 m/s with normal load ≥ 40.00 nN, and at the speed of 10 m/s with normal load ≥ 3.00 nN. This scratching type was characterised by a quick penetration of the grain into the material without adhered silica materials on the grain. The fast penetration produced by great normal force with less interaction time between atoms did not provided enough time for the optical glass material to adhere on grain. As a result of the high load force, the velocity of penetration in Z axis is higher than the horizontal sliding velocity. This provokes that the time of optical glass materials contact on the grain surface becomes shorter than the necessary time to adhere the silica on α -alumina. Therefore, it avoids the dragging phenomenon [16, 46].

When scratching at the speed of 100 m/s with normal load at 10.00 nN, 3.00 nN and 0.75 nN or at the speed of 10 m/s with the normal load of 0.75 nN, the dragging phenomenon happened along with the penetration. Fig.3.c shows an example. This penetration and dragging scratching type was featured by the lower penetration speed of the grain into the silica materials, the adhered silica on the α -alumina leading to silica material displacement. The lower load normal force leads to relatively slower penetration speed, which gives the sufficient time for the optical glass materials to adhere on the grain and to be dragged away [16, 46]. The adhesion only appeared after about 16 ps of scratching.

The scratchings under the normal load at 0.05 nN for both horizontal velocities of 100 m/s and 10 m/s shows dragging actions, featured by dragged material displacement and adhered material on the grain; Fig.3 (e, f) are examples. At this case, the normal force is insufficient to penetrate the optical glass materials, which provokes the horizontal interactions at the interface of the two materials. The adhered material amount is thus increased over the time.

All scratching created a structural modified zone in the silica materials under the grain. With the grain penetration, the altered zone is as a result of the plastic deformation caused by the high normal force [20, 21]. In the case of the dragging, this zone is produced by the molecular reorganisation of the surface atoms via adhesion effect [18]. The zone for penetration with drag-scratching is owing to both reasons because both processes can be found in these scratchings. The plastic deformation and adhesion effect were also found in the chemical phenomena, which will be discussed in 3.2. Section (Chemical Phenomena).

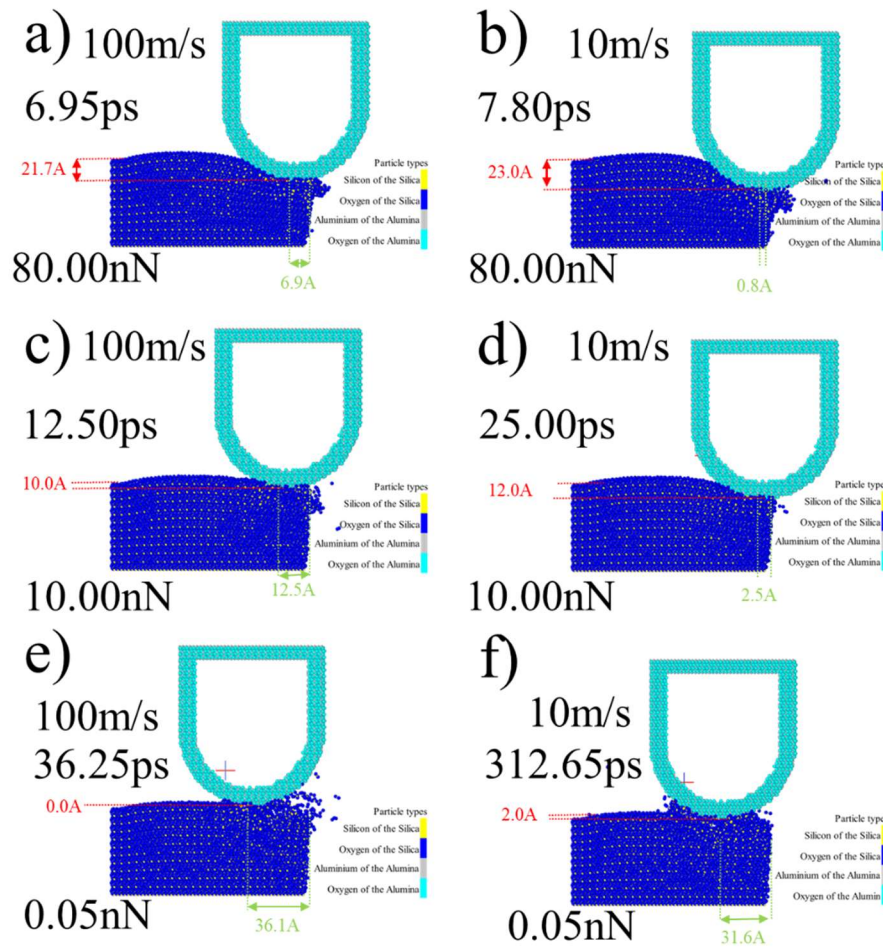


Figure.3. Ovito images of the fused silica scratching with α -alumina at 100m/s (a,c and e) and 10m/s (b, d and f) with 80.00nN (a-b), 10.00nN (c-d) and 0.05nN (e-f). Yellow particles are silicon of the silica, dark blue particles are the oxygen of the silica, grey particles are aluminium of the alumina and light blue particles are oxygen of the alumina.

A scratching process could be characterised by the depth and length of the scratching that the grain travel from the scratching starts to the point that the system becomes unstable. The influence of the normal force and velocity on these features can be viewed in Figure 4.

The penetration depth (Fig.4.a) was increased with the increase of the normal force and the decrease of the velocity. With higher normal force, the materials could be penetrated faster because structural strength is quickly exceeded [49]. The penetration depth in turn is proportional to this factor.

The scratching length before system unstable (Fig.4.b) was shorter at slower velocity and higher normal forces. The fast velocity obviously permits the scratching to cover longer distance than slow velocity, while the low normal force allows the systems stay in stable for longer time. The time that the force applied on a contact point of glass surface is inversely proportional to the velocity.

The dragging occurrence requires a certain interaction pressure and a certain time to establish. Therefore, lower normal load will allow system stay stable long enough for dragging to establish. It is noted that the dragging only appears when the normal load is lower than a certain value for a given speed. In this investigation, it shows the dragging will appear when the normal load is less than 10.00 nN for the sliding velocity equals to 100 m/s and when the normal load is less than 0.75 nN for the sliding velocity equals to 10 m/s.

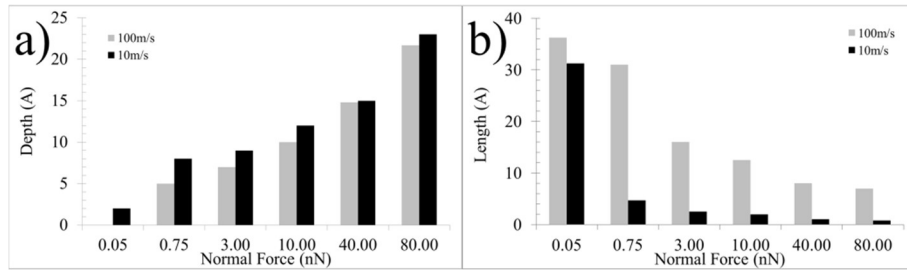
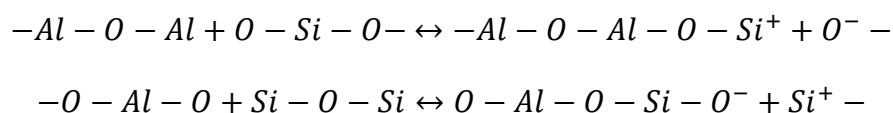


Fig. 4. Graphs of the scratching depth a) and horizontal displacement b) in function of normal force.

2. Chemical Phenomena

The chemical interactions of the scratching were studied through the assessment and the discussion of the simulation visualisation and chemical energy developments over time. These energies were according to bond, lone pair and torsion molecules. The variation of these energies over time indicated chemical interactions between the engaged bodies. The chemical interactions were the other essential part of scratching mechanisms.

The chemical interactions between fused silica (optical glass material) and α -alumina (abrasive grain) can be viewed in Figure 5. The main chemical interactions were between the oxygen of the silica and the aluminium of the alumina, and between the silicon of the silica with the oxygen of the alumina. This chemical interaction dragged the silica on the grain surface as shown in Figure 5 (indicated by red arrows), where the silica was adhered to grain surface by single or several molecules. These chemical interactions were observed by Lomic et al [50]. The chemical reaction mechanisms were proposed to these chemical interactions as:



The accumulation of the silica was seen on the optical glass material surface after grain sliding due to detached the silica adhered to α -alumina. The weakness of the adhesion bond could still allow the adhered silica to be easily broken.

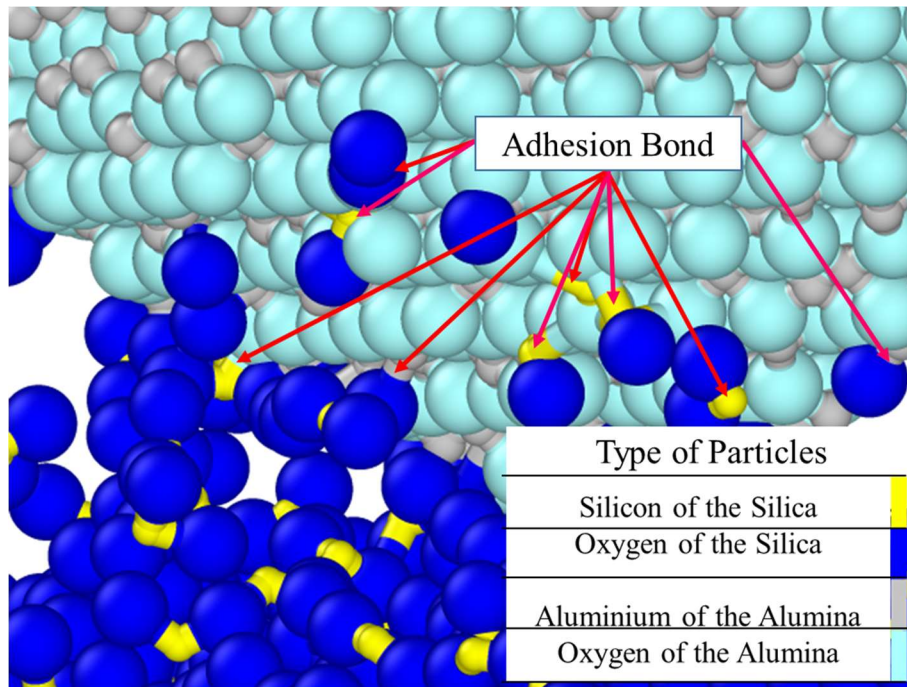


Figure.5. Observation of chemical reaction between abrasive grain and optical glass material at the scratching time 240 ps with the speed of 10m/s and normal force of 0.05n N applied.

The chemical energy developments over time of the simulations were evaluated to assess the chemical interactions in depth. Simulation chemical energies were dissimilar according to the velocities and normal forces (Fig.6-8).

The bond energy (Fig.6.) developed over time with dissimilar behaviour in according to the normal force and velocity. Similar to potential energy behaviours, the system destabilisation behaviours of the simulations were featured by the dramatic reduction of the bond energy because the massive destruction of the bonds [32-35].

Under the condition of velocity at 100 m/s, (Fig.6.a) showed the bond energy was observed in this kind. This is fluctuated due to the grain pressed on the optical glass material surface and reduced the bond length that increases the bond energy. When the atoms are so close, the interatomic repulsion forces increased to repel the atoms from each other, which in turn diminished the bond energy [51]. The fluctuation cycle is around 2 ps, which is equivalent to average atom distance for 100 m/s. Such energy fluctuation could last up to 16 ps. After this time, the bond energy became less fluctuated and reduced with the time increment until the system destabilisation point. This can be owing to the adhesion of the silica on α -alumina breaks strong bonds and generates weak bonds. This could indicate that the time the adhesion process establishment is ≈ 16 ps.

When the simulation velocity reduced to 10 m/s (Fig.6.b), the majority of simulations showed similar behaviours. The only exception was the simulation at the normal load of 0.05 nN. Bond energy evolution would stay relatively constant after 48 ps until 208 ps when a valley appeared in the end of the simulation. The constant energy shows the force of the

bonds remains constant over time [32-35]. The valley indicates an adhesion/detaching process between silica and alumina. The re-deposition or adsorption of these molecules on the materials diminished the bond energy via the replacing of the covalent (strong) bond by adhesion (weak) bonds. The fall of the silica adhered increased the bond energy via the creation of strong bonds with the materials [32-35]. Note, this valley was observed in the potential energy graph (Fig.2.b.) and coincided in the time with the peak of the temperature graph (Fig.2.a). This shows the thermodynamic effects of the adhesion/detaching process on the system.

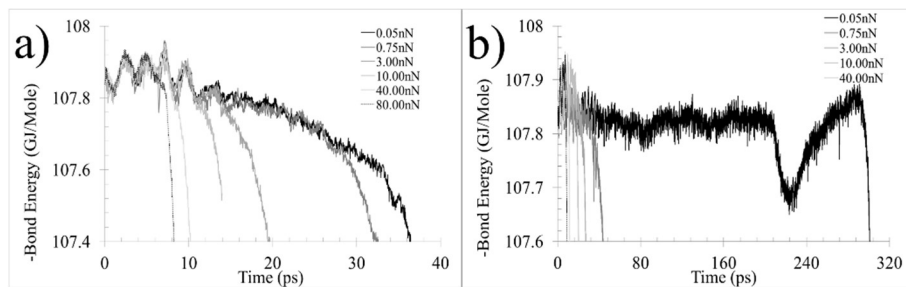


Figure.6. Graphs of the bond energy in function of time for the simulations at 100m/s (a) and at 10m/s (b).

The lone pair energy evolution over time (Fig.7.) was distinct for different normal forces and velocities but all destabilisation system point was featured with the same form that was the fast increment of the lone pair energy. The broken bond electrons are split between the atoms, which increases the non-bonding (lone pair) electrons number [32].

The simulation at the velocity of 100 m/s (Fig.7.a) owned two types of the energy evolution over time according to different normal forces. The simulation with normal load ≥ 40.00 nN possessed energy evolution that was featured by an increment of the energy with the time at first picoseconds. This first type of energy evolution is due to the plastic deformation of the optical glass material, which produces a microstructural change that further generates lone pair electrons through bond breaking. The lone pair energy will then diminish with the time increment until system destabilisation point owing to the deeper penetration of the abrasive grain into the optical glass material with these normal loads. The contact area between abrasive grain and the silica materials will increase with the depth of the scratching. The lone pair electrons of the bodies (abrasive grain and optical glass material) will in turn interact for each other to generate bonds, which will then reduce their lone pair electrons number. The second type of the lone pair energy development was found from the simulations at the normal load ≤ 10.00 nN. The first stage of this energy evolution was similar than that for the first type at the start of contact. After the first stage, the energy remained constant until the system destabilisation. This indicated that the number of the lone pair electrons are constant over the time [32] for this second stage. The adhesion is produced via the lone pair electrons of the surface molecules of the abrasive grain and optical glass

material. The adhesion of the silica molecules to α -alumina surface in turn is proportional to contact area. The dissimilarity of the energy evolution related to different normal forces is because of the different penetration of the grain. The limited penetration of the grain at low normal force (≤ 10.00 nN) provokes a limited contact area that provokes less changes in the lone pair energy due to the low lone pair electron interactions. In the opposite case, the contact area under higher normal force is increasing over time by the continuous penetration [48] and therefore, the abrasive grain and optical glass material lone pair electrons is increased.

In the case of the simulation at the velocity of 10 m/s (Fig.7.b), the first type of lone pair energy evolution was observed for simulations at the normal force ≥ 0.75 nN, whilst the second type was found for the simulations at the normal force at 0.05 nN. The first kind possessed the lone pair energy increment at low normal force than at great normal force because the less scratching depth. This produces a structural modified zone that owns high number of the lone pair electrons [52]. On the other hand, the lone pair energy reduction with the time was enlarged at greater normal force because of the higher penetration of the abrasive grain in the optical glass material. This provokes that the contact area is larger and therefore, more lone pair electrons are converted to bonding electrons. Although simulation at 0.005 nN showed similar evolution as the second type, the peak from 208 ps to 256p s was also seen. The pulling off of the silica molecules from the optical glass material by means of their adhesion to abrasive grain produces lone pair electrons due to the optical glass material bond breaking. This is observed as the up slope of the peak. The silica adhered on α -alumina will then be detached over time because of their weak bonds. The silica redeposited on surface will thereafter interact with the optical glass material molecules through the lone pair electrons. This reduces their number and this is represented as the down slope of the peak in the lone pair energy graph. The dissimilar lone pair energy evolution according to the normal force is a result of the same reason as that in the case of the simulation at 100 m/s [48].

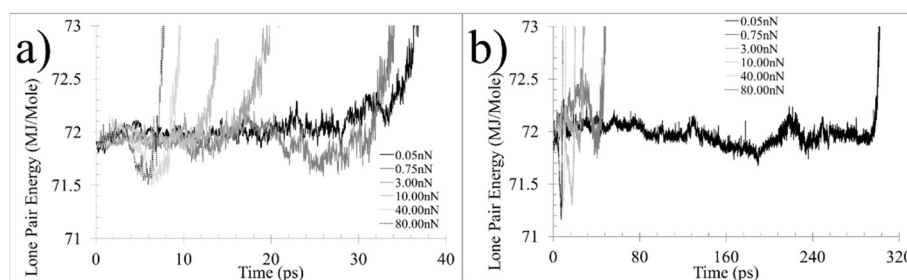


Figure.7. Graphs of the lone pair energy in function of time for the simulations at 100m/s (a) and at 10m/s (b).

Figures 8. shows that the torsion energy development over time was dissimilar according to the scratching conditions. The system destabilisation point nevertheless was

similar for all simulations that was characterised by the increment of the torsion energy. The generation of the single molecules through the material bond breaking have more movement freedom than the material molecules [53].

Two types of the energy evolution were found in the simulation at 100 m/s (Fig.8.a), which was depended of the normal force. The first type was at the normal force ≥ 3.00 nN, featured as the fluctuation of the energy until system destabilisation point. These fluctuations are owing to the structural changes produced by the optical glass material plastic deformation. This inserted pressure creates the enlargement and the shortening of the bonds. The twisting capacity of the molecules is reduced with the reduction of the bond length while the enlargement of the bond increases this capacity [36]. The second type of the energy evolution was observed in the simulation at the normal force ≤ 0.75 nN. The torsion energy evolution was similar to the first type when the scratching time ≤ 12 ps. After that, the torsion energy increased over the time until the point of system destabilisation because the adhered molecule number is enlarged with the time. The mobility capacity of the adhered silica molecule on α -alumina is higher than that for the silica molecule of the optical glass material. This can be considered another adhesion time that was dissimilar than previous time (16 ps). This is because the torsion energy can be more sensible to this adhesion process than the other chemical energies (bond and lone pair energy). Therefore, the initial adhesion time can be considered as 12 ps while the stable adhesion time can be defined as 16 ps.

Regarding the simulations at 10 m/s (Fig.8.b), the majority of the conditions had similar energy evolution than that for simulation at 100 m/s. The only exception was the simulation at 10 m/s and 0.05 nN. Before 12 ps, the energy evolution was similar to that for second type. From 12 ps to 32 ps, the energy remained constant with the time because the number of the silica adhered and detached are in a status of dynamic equilibrium. The energy then enlarged over time from 32 ps to 80 ps due to the amount of adhered silica molecules is increased with the grain displacement. The new equilibrium status between adhered/detached silica was found from 80 ps to 208 ps. A torsion energy peak was moreover observed before the system destabilisation point, as previous chemical and physical graphs. This peak is as a result of the accumulation of massive adhesion of the silica on α -alumina leading the increase of torsion energy. The torsion energy decreases when more silica detached from the abrasive grain owing to the larger compaction of the optical glass material silica than the silica molecules adhere on abrasive grain.

The dissimilar torsion energy behaviour depends on normal load on grain. High normal force reduces the time to system destabilisation while low force permits longer stable time. This permits to have larger interactions between the grain and the glass materials. In the case of the velocity, slower sliding will give longer stable time.

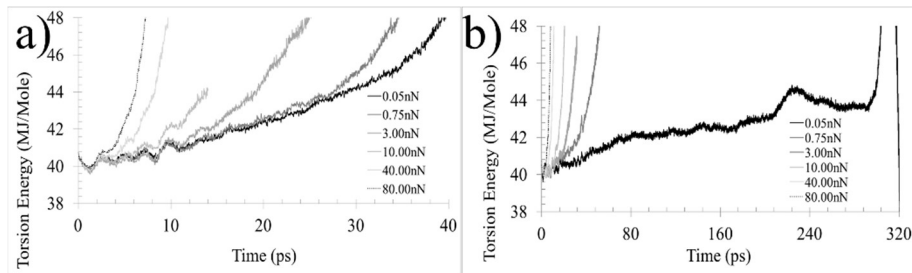


Figure.8. Graphs of the torsion energy in function of time for the simulations at 100m/s (a) and at 10m/s (b).

Conclusions

The molecular dynamics simulation has allowed the physical and chemical mechanisms of the silica surface scratching process with α -alumina abrasive to be assessed at nanoscale. The influence of acting normal force and abrasive velocity on material removal can be studied by using Reaxff force field in the simulation of the scratching processes of interests.

According to normal load and sliding velocity applied, the scratching actions can be classified as penetration (penetration without adhesion), penetration with dragging (penetration with adhesion) and dragging (non-penetration with adhesion). The structural changes of the optical glass material under the grain are due to the dislocation and plastic deformation. The simulation shows the formation of adhesion may require 12ps to start and 16 ps to establish.

The temperature and potential energy development over time are dissimilar according to the normal load and velocity. Higher force and faster velocities generate higher temperature and cause silica materials unstable in a shorter time.

The chemical interaction between α -alumina and silica is basically adhesion that is formed via none-bonding electrons. The energy evolution over time was dissimilar according to the normal load and velocity.

The simulations show that the scratching at the velocity of 10 m/s and the normal load of 0.05 nN possesses the longest stable time, therefore, to avoid surface damage lower velocity and normal load should be considered. In the future, the simulations with slower velocities (1 m/s and 0.33 m/s) will be to conducted to explore a more stable system for improving polishing performance.

References

1. Hartmann, P., et al., Optical glass and glass ceramic historical aspects and recent developments: a Schott view. *Applied Optics*, 2010. **49**(16): p. D157-D176.
2. Rajaramakrishna, R. and J. Kaewkhao, Glass material and their advanced applications. *KnE Social Sciences*, 2019. **2019**: p. kss. v3i18. 4769.

3. Li, M., et al., Study on the subsurface damage mechanism of optical quartz glass during single grain scratching. *Ceramics International*, 2021. **47**(6): p. 7683-7691.
4. Brinksmeier, E., et al., Ultra-precision grinding. *CIRP annals*, 2010. **59**(2): p. 652-671.
5. Zhang, Y., et al., Quality improvement of collimating lens produced by precision glass molding according to performance evaluation. *Optics Express*, 2019. **27**(4): p. 5033-5047.
6. Yi, A.Y. and A. Jain, Compression molding of aspherical glass lenses—a combined experimental and numerical analysis. *Journal of the American Ceramic Society*, 2005. **88**(3): p. 579-586.
7. Belkhir, N., D. Bouzid, and V. Herold, Surface behavior during abrasive grain action in the glass lapping process. *Applied surface science*, 2009. **255**(18): p. 7951-7958.
8. Suratwala, T.I., et al., Subsurface mechanical damage correlations after grinding of various optical materials. *Optical Engineering*, 2019. **58**(9): p. 092604.
9. Cumbo, M., et al., Slurry particle size evolution during the polishing of optical glass. *Applied Optics*, 1995. **34**(19): p. 3743-3755.
10. Doi, T.K., T. Kasai, and H.K. Tonshoff, *Lapping and polishing*, in *Handbook of Ceramic Grinding & Polishing*. 1999, Elsevier. p. 354-442.
11. Gu, W., Z. Yao, and K. Li, Evaluation of subsurface crack depth during scratch test for optical glass BK7. *Proceedings of the Institution of Mechanical Engineers, Part C: Journal of Mechanical Engineering Science*, 2011. **225**(12): p. 2767-2774.
12. Wan, Z., et al., Effect of scratch direction on densification and crack initiation of optical glass BK7. *Ceramics International*, 2020. **46**(10): p. 16754-16762.
13. Thonggoom, R. and P. Funkenbusch, Transition in material removal behavior during repeated scratching of optical glasses. *Journal of materials science*, 2005. **40**(16): p. 4279-4286.
14. Dong, Y., Q. Li, and A. Martini, Molecular dynamics simulation of atomic friction: A review and guide. *Journal of Vacuum Science & Technology A: Vacuum, Surfaces, and Films*, 2013. **31**(3): p. 030801.
15. Goel, S., et al., Diamond machining of silicon: a review of advances in molecular dynamics simulation. *International Journal of Machine Tools and Manufacture*, 2015. **88**: p. 131-164.
16. Nguyen, V.-T. and T.-H. Fang, Molecular dynamics simulation of abrasive characteristics and interfaces in chemical mechanical polishing. *Applied Surface Science*, 2020. **509**: p. 144676.
17. Tian, Z., et al., Study on nanomechanical properties of 4H-SiC and 6H-SiC by molecular dynamics simulations. *Ceramics International*, 2019. **45**(17): p. 21998-22006.
18. Han, X., Investigation on the complex interaction between particle and substrate in mechanical polishing of silica glass. *The International Journal of Advanced Manufacturing Technology*, 2016. **85**(9): p. 2567-2575.
19. Hollingsworth, S.A. and R.O. Dror, Molecular dynamics simulation for all. *Neuron*, 2018. **99**(6): p. 1129-1143.
20. Tian, Z., X. Chen, and X. Xu, Molecular dynamics simulation of the material removal in the scratching of 4H-SiC and 6H-SiC substrates. *International Journal of Extreme Manufacturing*, 2020. **2**(4): p. 045104.
21. Meng, B., D. Yuan, and S. Xu, Study on strain rate and heat effect on the removal mechanism of SiC during nano-scratching process by molecular dynamics simulation. *International Journal of Mechanical Sciences*, 2019. **151**: p. 724-732.

22. Zhang, P., et al., Influence of double-tip scratch and single-tip scratch on nano-scratching process via molecular dynamics simulation. *Applied surface science*, 2013. **280**: p. 751-756.
23. Wu, Z., L. Zhang, and S. Yang, Effect of abrasive grain position patterns on the deformation of 6H-silicon carbide subjected to nano-grinding. *International Journal of Mechanical Sciences*, 2021. **211**: p. 106779.
24. Shi, Z., et al., Interfacial friction properties in diamond polishing process and its molecular dynamic analysis. *Diamond and Related Materials*, 2019. **100**: p. 107546.
25. Guo, X., et al., Effects of pressure and slurry on removal mechanism during the chemical mechanical polishing of quartz glass using ReaxFF MD. *Applied Surface Science*, 2020. **505**: p. 144610.
26. Onodera, T., H. Takahashi, and S. Nomura, First-principles molecular dynamics investigation of ceria/silica sliding interface toward functional materials design for chemical mechanical polishing process. *Applied surface science*, 2020. **530**: p. 147259.
27. Wen, J., et al., Atomistic mechanisms of Si chemical mechanical polishing in aqueous H₂O₂: ReaxFF reactive molecular dynamics simulations. *Computational Materials Science*, 2017. **131**: p. 230-238.
28. Liu, J., et al., Reaction analysis and visualization of ReaxFF molecular dynamics simulations. *Journal of Molecular Graphics and Modelling*, 2014. **53**: p. 13-22.
29. Simulator, M.M.P., LAMMPS Users Manual. 2003.
30. Psfogiannakis, G.M., et al., ReaxFF reactive molecular dynamics simulation of the hydration of Cu-SSZ-13 zeolite and the formation of Cu dimers. *The Journal of Physical Chemistry C*, 2015. **119**(12): p. 6678-6686.
31. Stukowski, A., Visualization and analysis of atomistic simulation data with OVITO—the Open Visualization Tool. *Modelling and simulation in materials science and engineering*, 2009. **18**(1): p. 015012.
32. Mueller, A.C. and W.A. Goddard III, ReaxFF potential functions.
33. Van Duin, A.C., et al., ReaxFFSiO reactive force field for silicon and silicon oxide systems. *The Journal of Physical Chemistry A*, 2003. **107**(19): p. 3803-3811.
34. Russo Jr, M.F. and A.C. Van Duin, Atomistic-scale simulations of chemical reactions: Bridging from quantum chemistry to engineering. *Nuclear Instruments and Methods in Physics Research Section B: Beam Interactions with Materials and Atoms*, 2011. **269**(14): p. 1549-1554.
35. Fantauzzi, D., et al., Development of a ReaxFF potential for Pt–O systems describing the energetics and dynamics of Pt-oxide formation. *Physical Chemistry Chemical Physics*, 2014. **16**(42): p. 23118-23133.
36. Van Duin, A.C., et al., ReaxFF: a reactive force field for hydrocarbons. *The Journal of Physical Chemistry A*, 2001. **105**(41): p. 9396-9409.
37. Aswad, M., *Residual stress and fracture in high temperature ceramics*. 2012: The University of Manchester (United Kingdom).
38. Joshi, N., et al., Size effect on melting temperatures of alumina nanocrystals: molecular dynamics simulations and thermodynamic modeling. *Computational Materials Science*, 2018. **145**: p. 140-153.
39. Scherer, C., Molecular dynamics simulations of silicate and borate glasses and melts: structure, diffusion dynamics and vibrational properties. 2015, Mainz, Univ., Diss., 2015.
40. Ranjan, P., R. Balasubramaniam, and V. Jain, Mechanism of material removal during nanofinishing of aluminium in aqueous KOH: a reactive molecular dynamics simulation study. *Computational Materials Science*, 2019. **156**: p. 35-46.

41. O'donoghue, J. and A. Cameron, Friction and temperature in rolling sliding contacts. *ASLE TRANSACTIONS*, 1966. **9**(2): p. 186-194.
42. Hapkiewicz, A., Clarifying chemical bonding. *The Science Teacher*, 1991. **58**(3): p. 24.
43. Meng, B., Y. Zhang, and F. Zhang, Material removal mechanism of 6H-SiC studied by nano-scratching with Berkovich indenter. *Applied Physics A*, 2016. **122**(3): p. 1-9.
44. Chavoshi, S.Z. and S. Xu, Nanoindentation/scratching at finite temperatures: Insights from atomistic-based modeling. *Progress in Materials Science*, 2019. **100**: p. 1-20.
45. Shakhvorostov, D., K. Pöhlmann, and M. Scherge, An energetic approach to friction, wear and temperature. *Wear*, 2004. **257**(1-2): p. 124-130.
46. Chen, M.Y., et al. Effect of textured surface on sliding friction investigated using molecular dynamic simulation. in *Applied Mechanics and Materials*. 2013. Trans Tech Publ.
47. Delpierre, G. and B. Sewell, Temperature and Molecular Motion 2002-2005.
48. Zhang, Z., I. Alabd Alhafez, and H.M. Urbassek, Scratching an Al/Si interface: Molecular dynamics study of a composite material. *Tribology Letters*, 2018. **66**(3): p. 1-12.
49. Tseng, A.A., et al., Scratch direction and threshold force in nanoscale scratching using atomic force microscopes. *Applied Surface Science*, 2011. **257**(22): p. 9243-9250.
50. Lomić, G.A. and E.E. Kiss, Subtle interactions in silica-alumina mixtures. *Reaction Kinetics and Catalysis Letters*, 2008. **95**(1): p. 61-69.
51. Navabi, A.M., *Mechanical Characterization via Full Atomistic Simulation: Applications to Nanocrystallized Ice*. 2016: Northeastern University.
52. Agrawalla, S. and A.C. Van Duin, Development and application of a ReaxFF reactive force field for hydrogen combustion. *The Journal of Physical Chemistry A*, 2011. **115**(6): p. 960-972.
53. Gerber, T. and B. Himmel, The structure of silica glass. *Journal of non-crystalline solids*, 1986. **83**(3): p. 324-334.